Optimal Scheduling of FTPSS with PV and HESS Considering the Online Degradation of Battery Capacity

Minwu Chen, *Member, IEEE*, Zongyou Liang, Zhe Cheng, Jinyu Zhao, and Zhongbei Tian

***Abstract*—To improve the power quality (PQ) and eliminate the neutral zone (NZ), a flexible traction power supply system (FTPSS) was proposed to provide flexible interfaces for hybrid energy storage system (HESS) and photovoltaic (PV). However, in order to realize the optimal scheduling of FTPSS, it is necessary to further study the high cost of HESS and battery available capacity. In this study, a two-layer model with the lowest comprehensive cost as the goal is proposed, which includes the cost of investment, replacement, operation and maintenance (O&M), and electricity. In the upper layer, the HESS sizing and replacement strategy are performed to achieve the lowest daily comprehensive cost within the project period. In the lower layer, based on the piecewise linear method, the battery capacity degradation is formulated as a linear mathematical model concerning the depth of discharge (DOD). Then, with the aim to achieve the lowest electricity charge, a mixed-integer linear programming (MILP) model is formulated by associating PV, regenerative braking energy (RBE) and HESS. Sparrow search algorithm (SSA) with CPLEX solver embedded is utilized to solve this two-layer nonlinear model. Finally, the simulation results show that the proposed model can achieve 13.55% cost reduction.**

***Index Terms*—Flexible traction power supply system, hybrid energy storage system, mixed-integer linear programming, battery capacity degradation online model.**

NOMENCLATURE

A. Abbreviations, Indices and Sets

PQ	Power quality
NZ	Neutral zone
FTPSS	Flexible traction power supply system
HESS	Hybrid energy storage system
PV	Photovoltaic
O&M	Operation and maintenance
DOD	Depth of discharge
MILP	Mixed-integer linear programming
RBE	Regenerative braking energy
SSA	Sparrow search algorithm
TPSS	Traction power supply system
RFCM	Rain-flow counting method
CPTC	Co-phase traction converter
GA	Genetic algorithm
GWO	Grey wolf optimization
SOC	State of charge
PCS	Power conversion systems
BOP	Balance of Plant
ECC	Energy consumption charge
DMC	Demand charge
PC	Penalty charge
TOU	Time-of-use
MPSO	Modified particle swarm optimization

B. Parameters

T_{pro}	Project period (year)
$k_{\mathrm{P}}^{\mathrm{bat}}$, $k_{\mathrm{P}}^{\mathrm{uc}}$	Unit power cost of battery and UC (CNY/kW)
$k_{\mathrm{E}}^{\mathrm{bat}}$, $k_{\mathrm{E}}^{\mathrm{uc}}$	Unit capacity cost of battery and UC (CNY/kWh)
$k_{\mathrm{rep}}^{\mathrm{Ebat}}$, $k_{\mathrm{rep}}^{\mathrm{Euc}}$	Unit replacement cost of the capacity associated with battery and UC (CNY/kWh)
$k_{\mathrm{om,f}}^{\mathrm{bat}}$, $k_{\mathrm{om,f}}^{\mathrm{uc}}$	Unit fixed O&M cost (CNY/kW/year)
$k_{\mathrm{om,v}}^{\mathrm{bat}}$, $k_{\mathrm{om,v}}^{\mathrm{uc}}$	Unit variable O&M cost (CNY/kW/h)
$\lambda_{\mathrm{dep}}^{\mathrm{bat}}$, $\lambda_{\mathrm{dep}}^{\mathrm{uc}}$	Depreciation coefficient for the recovery of battery banks and UC banks
r_0	Annual discount rate
$P_{\mathrm{low}}^{(\cdot)}$, $P_{\mathrm{up}}^{(\cdot)}$	Lower and upper bounds of battery or UC power rating (WM)
$E_{\mathrm{low}}^{(\cdot)}$, $E_{\mathrm{up}}^{(\cdot)}$	Lower and upper bounds of battery or UC capacity rating (MWh)
$(\cdot)$	Battery or UC
π_s	Probability of PV generation scenario
$p_{t,s}$	Electricity price for power imported from the utility grid (CNY/kWh)
$p_{t.s}^{\mathrm{dem}}$	Electricity price of peak demand power (CNY/kWh)
p_{pv}	Unit O&M cost of PV (CNY/kWh)

This paper has been partially supported by funding of the National Natural Science Foundation of China under Grant 51877182 and Chengdu Guojia Electrical Engineering Co., Ltd (No. NEEC-2019-B04). (*Corresponding author: Zongyou Liang.*)

M. Chen, Z. Liang, Z. Cheng and J. Zhao are with National Rail Transportation Electrification and Automation Engineering Technology Research Centre, Chengdu 610031, China. They are also with the School of Electrical Engineering, Southwest Jiaotong University, Chengdu, Sichuan, 611756, China. (e-mail: chenminwu@home.swjtu.edu.cn; 2435828243@my.swjtu.edu.cn; chengzhe@my.swjtu.edu.cn; Jinyu_Zhao30@my.swjtu.edu.cn)

Z. Tian is with the Department of Electrical Engineering and Electronics, University of Liverpool, Liverpool, U.K. (e-mail: Zhongbei.tian@liverpool.ac.uk).

N_{cycle} Number of life cycles
L_{bat} Battery lifetime (year)
L_{uc} UC lifetime (year)
$N_{\text{rep}}^{\text{bat}}$ Number of battery replacement
$N_{\text{rep}}^{\text{uc}}$ Number of UC replacement
$C_{\text{HESS}}^{\text{cap}}$ HESS daily capital cost
$C_{\text{HESS}}^{\text{rep}}$ HESS daily replacement cost
$C_{\text{HESS}}^{\text{om}}$ HESS daily O&M cost
C_{e} Daily electric cost
C^{pv} PV daily O&M cost
C_{sal} HESS salvage daily cost
C_{total} Total daily cost
T Number of samples
Δt Sampling time interval (1 min)
P_t^{brake}, P_t^{load} Braking and tractive power (MW)
$\eta_{\text{dis}}^{\text{bat}}$, $\eta_{\text{ch}}^{\text{bat}}$ Discharge and charge efficiency of battery
$\eta_{\text{dis}}^{\text{uc}}$, $\eta_{\text{ch}}^{\text{uc}}$ Discharge and charge efficiency of UC
ε_{bat}, ε_{uc} Battery and UC self-discharge rate
$SOC_{\text{min}}^{\text{bat}}$ Minimum values of battery SOC
$SOC_{\text{max}}^{\text{bat}}$ Maximum values of battery SOC
$SOC_{\text{min}}^{\text{uc}}$ Minimum values of UC SOC
$SOC_{\text{max}}^{\text{uc}}$ Maximum values of UC SOC
SOC_0^{bat} Initial SOC of the battery
SOC_0^{uc} Initial SOC of the UC
S^{pv} PV converter capacity (MW)
$F_{t,s}^{\text{pv}}$ Solar intensity (kW/m^2)
$P_{\text{lim}}^{\text{grid}}$ Maximum limit for power from grid (MW)
$P_{\text{lim}}^{\text{fed}}$ Maximum limit for power fed back to grid (MW)
η_{pv} Efficiency of PV generation
A_{pv} Total area of PV panels (m^2)

C. Variables

$P_{\text{rate}}^{\text{bat}}$, $P_{\text{rate}}^{\text{uc}}$ Rated capacity of the battery and UC (MW)
$E_{\text{rate}}^{\text{bat}}$, $E_{\text{rate}}^{\text{uc}}$ Rated power of the battery and UC (MWh)
$T_{\text{op}}^{\text{bat}}$, $T_{\text{op}}^{\text{uc}}$ Daily operating time of battery and UC
$P_{t,s}^{\text{grid}}$ Power supplied from grid (MW)
$P_{t,s}^{\text{fed}}$ Power fed back to grid (MW)
$P_{t,s}^{\text{pv}}$ Power input from the PV power generation systems to FTPSS (MW)
P_t^{bake}, P_t^{load} Braking and tractive power (MW)
$P_{t,s}^{\text{bat,ch}}$, $P_{t,s}^{\text{uc,ch}}$ Battery and UC charge power (MW)
$P_{t,s}^{\text{bat,dis}}$, $P_{t,s}^{\text{uc,dis}}$ Battery and UC discharge power (MW)
$D_{t,s}^{\text{bat}}$ Cycle depth
$E_{t,s}^{\text{bat,st}}$, $E_{t,s}^{\text{uc,st}}$ The energy stored in battery and UC (MWh)
$E_{t,s}^{\text{bat,act}}$ Actual battery capacity (MWh)
$O_{t,s}^{\text{bat,ch}}$, $O_{t,s}^{\text{uc,ch}}$ Binary variable: 1 if battery or UC charge, 0 otherwise
$O_{t,s}^{\text{bat,dis}}$ Binary variable: 1 if battery or UC discharge, 0 otherwise
$O_{t,s}^{\text{uc,dis}}$ Binary variable: 1 if battery or UC discharge, 0 otherwise
$O_{t,s}^{\text{grid}}$ Binary variable: 1 if power is supplied from grid, 0 if power is fed back to grid

I Introduction

In the traditional 27.5kV AC traction power supply system (TPSS), the PQ problem dominated by negative sequence is becoming more and more serious [1]. As shown in Fig. 1, speed loss and overvoltage problems will occur when electric trains pass through NZ, which not only reduces the power supply efficiency and quality, but also affects the economy of railway operation [2]. In addition, the rapid development of China's railway is also facing new challenges. Taking Sichuan-Tibet Railway as an example, the slope of 30% ramps is greater than 300km, and a lot of RBE is generated during train braking, which cannot be effectively utilized. At the same time, western China is rich in solar energy resources, but the utilization of PV power generation along the railway is low. As shown in Fig.2, the proposal of FTPSS [3-5] can solve the above problems and provide flexible interfaces for HESS and PV [6].

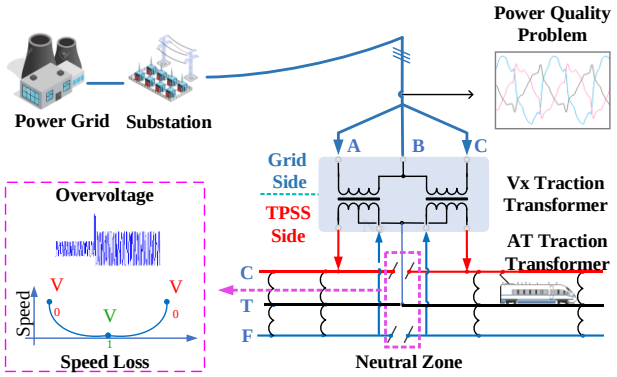

Fig. 1. The structure diagram of the traditional TPSS.

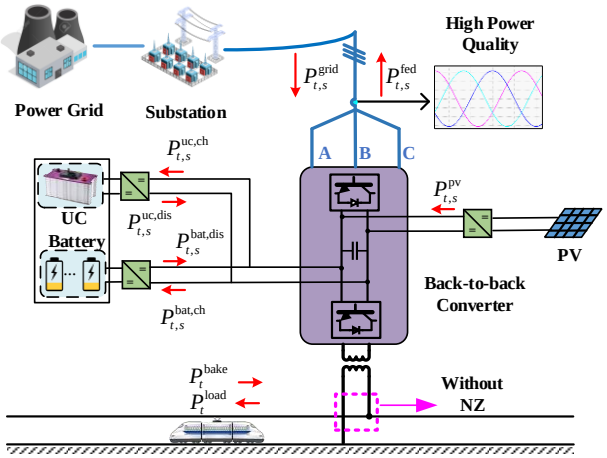

Fig. 2. The structure diagram of the FTPSS.

HESS is widely applied to recover RBE [7-12], but it is mainly about energy storage access rather than the energy management of the whole TPSS. Reference [13] proposed a hierarchical coordination model which focused on the improvement of energy and cost-efficiency of TPSS concerning real train parameters and timetables. The HESS was employed to reduce the TPSS operating costs and achieve the effective performance. In reference [14] and [15], the energy management models for optimal operation of TPSS considering renewable energy, RBE and HESS were proposed, and case studies showed that the HESS can improve the utilization rate of renewable energy and RBE. However, the cost of investment, replacement, operation and maintenance of HESS was ignored, which was key for the optimization of energy management.

In FTPSS, DC link provides better access for HESS and PV. How to coordinate the power flow control of back-to-back converter is critical for the optimization scheduling. In reference [16], the rain-flow counting method (RFCM) was adopted and a hierarchical model considering diurnal scheduling of converter was proposed. Reference [17] proposed a multi-time scale optimization model, which realized the day-ahead optimal scheduling of back-to-back converters, HESS and PV, and modified day-ahead scheduling in the intra-day stage. Reference [18] proposed a two-stage model for the flexible control of co-phase traction converter (CPTC) with the integration of PV and HESS. The first stage determined the operating state of HESS and the converter, and the second stage aimed to find the optimal scheduling of CPTC in the worst-case scenario. In the filed application, the dynamical degradation characteristics of the battery have drawn more attention and the available capacity of the battery was decreased under different traction and regeneration condition [19].

Actually, the lifetime model of HESS including the comprehensive cost is nonlinear. Intelligent algorithm can provide effective solutions for engineering application[20-22]. In reference [23], the genetic algorithm (GA) was used to optimize the train control strategy so as to reduce the energy consumption of the train during the specified running time. In order to solve the large-scale nonlinear model proposed in reference [16], the grey wolf optimization (GWO) was adopted. However, the intelligent algorithm also has its limitations such as its optimization result may be the local optimal value, solving some models even do not converge, these are also problems that scholars are trying to solve. Reference [24] proposed SSA, and combining with case analysis, it is proved that SSA has faster convergence speed and higher precision than GWO and other algorithms.

Accordingly, this paper aims at providing an insight into these problems. The main contributions of this paper are addressed as follows:

(i) A novel two-layer scheduling model for FTPSS including the HESS and PV is developed. HESS configuration parameters and comprehensive cost are optimized at the upper level, and power dispatch is performed to minimize the railway operation cost at the lower layer.

(ii) A piecewise linearization model is proposed to describe the degradation of battery capacity, which can effectively reduce the complexity of the model and improve computational accuracy.

(iii) A SSA with CPLEX solver embedded is proposed to solve the proposed two-layer model, which has higher accuracy and faster convergence speed.

The rest of this paper is organized as follows. Section 2 introduces the PV uncertainty model and HESS lifetime model. Section 3 presents the equations of the two-layer model for FTPSS energy management. Section 4 introduces the method of SSA with CPLEX solver embedded. Section 5 performs the case study and the conclusions are reached in section 6.

II. PV Uncertainty and HESS Lifetime Modeling

A. The Model of PV Uncertainty

The PV power generation system is mainly composed of PV panels, PV inverters and controllers, which can convert solar energy into electric energy and realize grid connection. Therefore, PV power is restricted by PV panels and PV inverters. In addition, considering the intermittency and volatility of PV, it is necessary to model the uncertainty of PV. In this paper, the scenario reduction algorithms [25] is applied to form a typical scene so as to achieve both computational efficiency and precision. Take the annual solar intensity data of a certain place as an example [17], the daily PV data vary widely, as shown in Fig. 3(a). Fig. 3(b) shows that four typical scenarios will be generated and the probability of each scenario will be obtained when the scenario reduction method is employed.

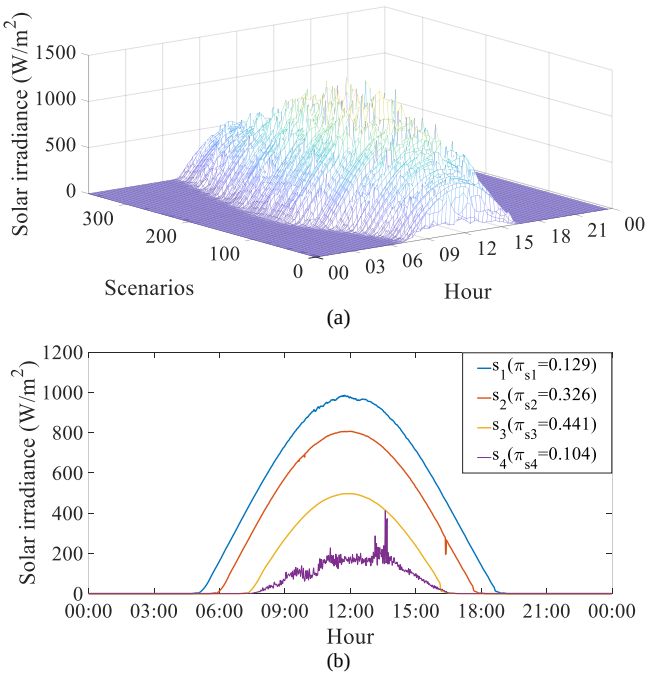

Fig. 3. Initial and reduced scenarios: (a) Annual data of solar irradiance; (b) Typical scenarios of solar irradiance after scenario reduction.

B. The Model of HESS Lifetime

Battery aging includes calendar aging and cycle aging. Calendar aging is affected by the temperature and the state of charge (SOC) of the battery. At constant temperature and SOC, calendar aging and time can be approximately linear. Two metrics can be used to assess the degradation of battery life. One is the aging of cycle life, and the other is the capacity wear, which accounts for the available energy [26]. This paper mainly focuses on the cycling conditions that have a great impact on

battery lifetime, such as frequent charging and discharging times and DOD of each cycle [27]. The DOD of each cycle is calculated by RFCM [28]. The principle of the RFCM is presented in Fig. 4. The process of discerning the full cycles and half cycles by RFCM is shown in Fig. 5. First, the peak and valley values of the daily SOC of the battery are found, and then the full cycle and half cycle are extracted. Next, DOD corresponding to each charge and discharge cycle is calculated, and the battery lifetime is obtained through the calculation of (1) - (4). Considering the effect of temperature on the battery lifetime [29], a constant operating temperature of 25℃ is assumed in this study.

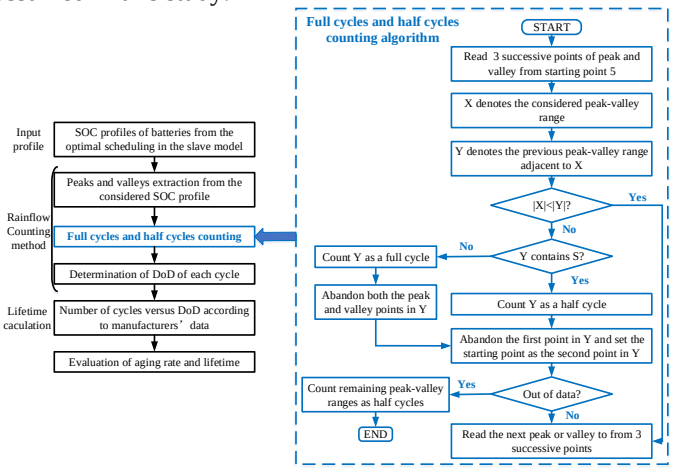

Fig. 4. Flow chart of battery aging rate and lifetime evaluation.

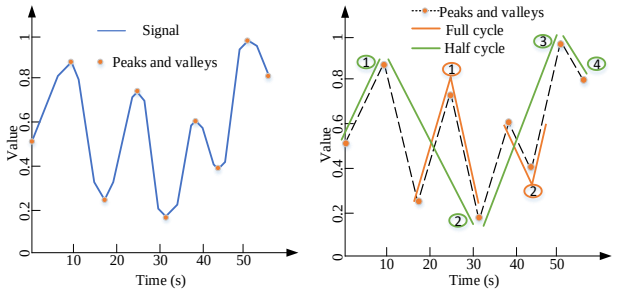

(a) (b)

Fig. 5. Demonstration of RFCM: (a) Extraction of peaks and valleys; (b) Discernment of full cycles and half cycles.

According to the data provided by manufacturers, the relationship between N_{cycle} and DOD of each cycle are fitted to (1) by applying least square interpolation. The parameters α, β, γ and ω are 24090, -9.346, 6085 and -1.319 respectively.

$$N_{\text{cycle}} = \alpha e^{\beta \cdot DOD} + \gamma e^{\omega \cdot DOD} \tag{1}$$

In order to make connections between L_{bat} and N_{cycle}, the accumulated aging rate A_{RATE} is formulated in (2) by summing up the aging rate of each cycle. Therefore, the battery lifetime can be expressed in (3).

$$A_{\text{RATE}} = \sum_{i=1}^{N} \frac{1}{N_{\text{cycle}}} \tag{2}$$

$$L_{\text{bat}} = \frac{1}{365 A_{\text{RATE}}} \tag{3}$$

$$N_{\text{rep}}^{\text{bat}} = \left\lfloor \frac{365 \cdot T_{\text{pro}}}{L_{\text{bat}}} \right\rfloor \tag{4}$$

where $\lfloor\ \rfloor$ represents round down to an integer operand.

The lifetime of a UC mainly depends on the principal function of temperature and terminal voltage [30]. And charging and discharging rates have little effect on UC degradation. The number of lifecycle and lifetime of UC are not limited by the DOD of each cycle [31]. In this study, it is believed that UCs are always working under rated conditions provided by the manufacturing specifications. Therefore, it is assumed that the value of the UC lifetime is equal to the number given in the manufacturing specification [29]. The number of UC replacement is constant during the fixed project time and can be formulated in (5). The capacity of UC is considered constant and rated.

$$N_{\text{rep}}^{\text{uc}} = \left\lfloor \frac{T_{\text{pro}}}{L_{\text{uc}}} \right\rfloor \tag{5}$$

III. Two-Layer Model for FTPSS Energy Management

A two-layer model aiming at the lowest total cost in the project period is proposed in this study, as illustrated in Fig. 6. At the upper level, taking the UC and battery degradation into account, a nonlinear model is established to minimize the comprehensive cost, which is composed of the investment cost, the operation and maintenance cost, the replacement cost, the electric charge, and the salvage cost. The configuration parameters of HESS are obtained through SSA. Among them, battery life is obtained by the RFCM, and UC degradation cost mathematical model is established. As shown in Fig. 6, the SOC related to battery life is derived from FTPSS scheduling model at the lower layer, and HESS O&M time and electricity cost are also calculated at the lower layer.

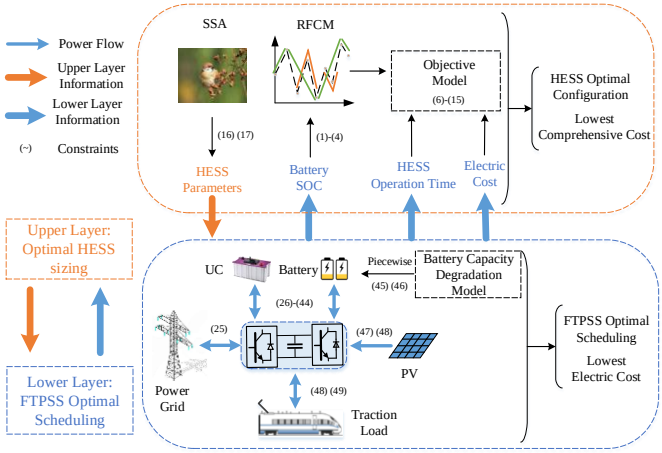

Fig. 6. Two-layer optimization model

At the lower layer, the online degradation model of battery capacity is established on account of the DOD and linearized by piecewise linearization method. According to the HESS parameters generated by SSA, the lowest daily electricity charge is derived and passed to the upper layer by establishing a series of constraint functions. Then, based on the PV prediction data and the measured traction load data, the power scheduling plan is achieved every minute. Besides, the operation hours of UC and battery included in the O&M cost function are transferred to the upper layer.

In brief, the upper layer focuses on the overall cost within the

project lifecycle and optimal sizing of HESS, and the lower layer plans the daily scheduling of FTPSS. In the two-layer model, the lowest daily comprehensive cost, the optimal parameters of HESS, and the optimal scheduling of FTPSS are interactively obtained through SSA with CPLEX embedded.

A. Upper Layer: Objective Function

Equation (6) represents the objective function of the upper model:

$$\begin{cases} \min\ f_1(x) = C_{\text{total}} = C_{\text{HESS}}^{\text{cap}} + C_{\text{HESS}}^{\text{rep}} + C_{\text{HESS}}^{\text{com}} + C_{\text{e}} - C_{\text{sal}} \\ x = [P_{\text{rate}}^{\text{bat}}, E_{\text{rate}}^{\text{bat}}, P_{\text{rate}}^{\text{uc}}, E_{\text{rate}}^{\text{uc}}] \end{cases} \tag{6}$$

The HESS provided by manufacturers consists of battery banks, UC banks, power conversion systems (PCS) and other devices related to the Balance of Plant (BOP). The cost of PCS is included in the cost of battery and UC. Equation (7) represents the investment cost of HESS, and (8) expresses the cost of devices related to BOP.

$$\begin{aligned} C_{\text{HESS}}^{\text{cap}} = \frac{CRF(r_0, T_{\text{pro}})}{365} (k_{\text{P}}^{\text{bat}} \cdot P_{\text{rate}}^{\text{bat}} \\ + k_{\text{E}}^{\text{bat}} \cdot E_{\text{rate}}^{\text{bat}} + k_{\text{P}}^{\text{uc}} \cdot P_{\text{rate}}^{\text{uc}} + k_{\text{E}}^{\text{uc}} \cdot E_{\text{rate}}^{\text{uc}} + C_{\text{BOP}}) \end{aligned} \tag{7}$$

$$C_{\text{BOP}} = k_{bop}(P_{\text{rate}}^{\text{bat}} + P_{\text{rate}}^{\text{uc}}) \tag{8}$$

The replacement cost for HESS is presented in (9). The O&M cost includes the fixed O&M cost and the variable O&M cost, which can be expressed as (10) to (12). At the end of the engineering cycle, the battery may not reach the life cycle of recycling, which is the salvage value expressed by (13).

$$\begin{aligned} C_{\text{HESS}}^{\text{rep}} = \frac{CRF(r_0, T_{\text{pro}})}{365} \\ \times [\sum_{i=1}^{N_{\text{rep}}^{\text{bat}}} (k_{\text{rep}}^{\text{Ebat}} \cdot E_{\text{rate}}^{\text{bat}}) + N_{\text{rep}}^{\text{uc}} \cdot k_{\text{rep}}^{\text{Euc}} \cdot E_{\text{rate}}^{\text{uc}}] \end{aligned} \tag{9}$$

$$C_{\text{HESS}}^{\text{om}} = C_{\text{HESS}}^{\text{om,f}} + C_{\text{HESS}}^{\text{om,v}} \tag{10}$$

$$C_{\text{HESS}}^{\text{om,f}} = \frac{1}{365} \times (k_{\text{om,f}}^{\text{bat}} \cdot P_{\text{rate}}^{\text{bat}} + k_{\text{om,f}}^{\text{uc}} \cdot P_{\text{rate}}^{\text{uc}}) \tag{11}$$

$$C_{\text{HESS}}^{\text{om,v}} = T_{\text{op}}^{\text{bat}} \cdot k_{\text{om,v}}^{\text{bat}} \cdot P_{\text{rate}}^{\text{bat}} + T_{\text{op}}^{\text{uc}} \cdot k_{\text{om,v}}^{\text{uc}} \cdot P_{\text{rate}}^{\text{uc}} \tag{12}$$

$$\begin{aligned} C_{\text{sal}} = \frac{(N_{\text{rep}}^{\text{bat}} + 1) \cdot L_{\text{bat}} - T_{\text{pro}}}{365 L_{\text{bat}}} \\ \times \lambda_{\text{dep}}^{\text{bat}} \cdot k_{\text{rep}}^{\text{Pbat}} \cdot P_{\text{rate}}^{\text{bat}} \cdot SFF(r_0, T_{\text{pro}}) \end{aligned} \tag{13}$$

CRF represents the capital recovery factor. *SFF* denotes the sinking fund factor. Both are related to the annual discount rate r_0 and T_{pro}, expressed as follows:

$$CRF(r_0, T_{\text{pro}}) = \frac{r_0 (r_0 + 1)^{T_{\text{pro}}}}{(r_0 + 1)^{T_{\text{pro}}} - 1} \tag{14}$$

$$SFF(r_0, T_{\text{pro}}) = \frac{r_0}{(r_0 + 1)^{T_{\text{pro}}} - 1} \tag{15}$$

B. Upper Layer: Constraint Functions

According to the objective function, the total cost is related to $P_{\text{rate}}^{\text{bat}}$, $E_{\text{rate}}^{\text{bat}}$, $P_{\text{rate}}^{\text{uc}}$ and $E_{\text{rate}}^{\text{uc}}$. Equations (16) and (17) state that the upper and lower boundaries of these decision variables are determined by the types of HESS and the traction load. Besides, (2) to (6) are also parts of the constraints of the upper level.

$$P_{\text{low}}^{(\cdot)} \le P_{\text{rate}}^{(\cdot)} \le P_{\text{up}}^{(\cdot)} \tag{16}$$

$$E_{\text{low}}^{(\cdot)} \le E_{\text{rate}}^{(\cdot)} \le E_{\text{up}}^{(\cdot)} \tag{17}$$

C. Lower Layer: Objective Function

The lower level model mainly focuses on the electricity which is composed of energy consumption charge (ECC) C^{ECC}, demand charge (DMC) C^{DEM} and penalty charge (PC) C^{PEN}. The energy consumption charge represents the electrical energy provided by the utility grid to the TPSS. DMC is related to the maximum average value of active power for 15 consecutive minutes during a day [32]. Besides, the traction load produces a lot of RBE in the braking stage. Part of RBE is used by the traction load and the rest is returned to the grid. The RBE returned to the power grid contains a lot of harmonics, which is not conducive to the normal operation of the power grid. Therefore, railway operators should pay penalties to the utility grid.

$$C_{\text{e}} = \text{C}^{\text{ECC}} + \text{C}^{\text{DEM}} + \text{C}^{\text{PEN}} + C^{\text{pv}} \tag{18}$$

$$C^{\text{ECC}} = \sum_s \pi_s \left(\sum_{t=1}^{T} p_{t,s} \cdot P_{t,s}^{\text{grid}} \cdot \Delta t \right) \quad \forall t, s \tag{19}$$

$$\begin{aligned} C^{\text{DEM}} = \sum_s [\pi_s \cdot p_{t.s}^{\text{dem}} \cdot \frac{\max(\sum_{t=1}^{t+14} P_{t,s}^{\text{grid}})}{15}] \\ \forall s \quad \forall t = 1, 2, ..., T - 14 \end{aligned} \tag{20}$$

$$C^{\text{PEN}} = \sum_s \pi_s \left(\sum_{t=1}^{T} p_{t,s} \cdot P_{t,s}^{\text{fed}} \cdot \Delta t \right) \quad \forall t, s \tag{21}$$

$$C^{\text{pv}} = \sum_s \sum_{t=1}^{T} (\pi_s \cdot p_{\text{pv}} \cdot P_{t,s}^{\text{pv}} \cdot \Delta t) \tag{22}$$

In order to make (20) linearized, it is transformed into (23) and (24) by introducing a new variable P_s^{peak}.

$$C^{\text{DEM}} = \sum_s (\pi_s \cdot p_{t.s}^{\text{dem}} \cdot P_s^{\text{peak}}) \quad \forall t, s \tag{23}$$

$$P_s^{\text{peak}} \ge P_{t,s}^{\text{dem}} \quad \forall s \ \forall t = 1, 2, ..., T - 14 \tag{24}$$

D. Lower Layer: Constraint Functions

In the FTPSS, energy conservation needs to be guaranteed, which can be expressed by (25).

$$\begin{aligned} P_{t,s}^{\text{grid}} + P_{t,s}^{\text{pv}} + P_{t,s}^{\text{bat,dis}} + P_{t,s}^{\text{uc,dis}} + P_t^{\text{brake}} \\ = P_t^{\text{load}} + P_{t,s}^{\text{bat,ch}} + P_{t,s}^{\text{uc,ch}} + P_{t,s}^{\text{fed}} \quad \forall t, s \end{aligned} \tag{25}$$

This study mainly focuses on battery capacity degradation, which is related to the cycle depth and charge moved [33]. The charge moved refers to the amount of electricity in and out of the battery during charging and discharging. And the incomplete invertibility of side reaction is the main cause for permanent battery capacity degradation [34]. The battery cycle loss and cycle depth $D_{t,s}^{\text{bat}}$ relate to a near-quadratic function [35]:

$$c(D_{t,s}^{\text{bat}}) = (5.24 \times 10^{-4}) \cdot (D_{t,s}^{\text{bat}})^{2.03} \quad \forall t, s \tag{26}$$

The reasonable assumptions of DODs were made to build the battery capacity degradation model with different DODs. Firstly, battery degradation is considered as a linear process [36]. Secondly, under different SOC levels, the battery capacity

degradation is considered to be the same as long as the depth of charging and discharging is the same. Based on these two assumptions, DOD in per unit time interval can be represented by (27).

$$D_{t,s}^{\text{bat}}=\frac{\frac{1}{\eta_{\text{dis}}^{\text{bat}}}\cdot P_{t,s}^{\text{bat,dis}}+\eta_{\text{ch}}^{\text{bat}}\cdot P_{t,s}^{\text{bat,ch}}}{E_{\text{rate}}^{\text{bat}}}\cdot\Delta t\quad\forall t,s \tag{27}$$

Therefore, the recursive formula of actual battery capacity $E_{t,s}^{\text{bat,act}}$ can be expressed as (28) and (29). Since the energy stored cannot mutate, the energy storage $E_{t,s}^{\text{bat,st}}$ and $E_{t,s}^{\text{uc,st}}$ at adjacent moments will have the constraint relationship as shown in (30) and (31).

$$E_{t=1,s}^{\text{bat,act}}=E_{\text{rate}}^{\text{bat}} \tag{28}$$

$$E_{t+1,s}^{\text{bat,act}}=E_{t,s}^{\text{bat,act}}-0.2E_{\text{rate}}^{\text{bat}}\cdot c(D_{t,s}^{\text{bat}})\quad\forall t,s \tag{29}$$

$$\begin{aligned}E_{t+1,s}^{\text{bat,st}}=&(1-\varepsilon_{\text{bat}})\cdot E_{t,s}^{\text{bat,st}}-\\&(\frac{1}{\eta_{\text{dis}}^{\text{bat}}}\cdot P_{t,s}^{\text{bat,dis}}+\eta_{\text{ch}}^{\text{bat}}\cdot P_{t,s}^{\text{bat,ch}})\cdot\Delta t\quad\forall t,s\end{aligned} \tag{30}$$

$$\begin{aligned}E_{t+1,s}^{\text{uc,st}}=&(1-\varepsilon_{\text{uc}})\cdot E_{t,s}^{\text{uc,st}}\\&-(\frac{1}{\eta_{\text{dis}}^{\text{uc}}}\cdot P_{t,s}^{\text{uc,dis}}+\eta_{\text{ch}}^{\text{uc}}\cdot P_{t,s}^{\text{uc,ch}})\cdot\Delta t\quad\forall t,s\end{aligned} \tag{31}$$

Equations (32) and (33) limit the SOC of HESS to avoid over-discharge and extend the lifetime of HESS. These boundaries can be obtained from the manufacturing specification. Equations from (34) to (36) set the start and end values of energy storage equal to make HESS diurnal, since this study focuses on daily power scheduling.

$$SOC_{\text{min}}^{\text{bat}}\cdot E_{t,s}^{\text{bat,act}}\le E_{t,s}^{\text{bat,st}}\le SOC_{\text{max}}^{\text{bat}}\cdot E_{t,s}^{\text{bat,act}}\quad\forall t,s \tag{32}$$

$$SOC_{\text{min}}^{\text{uc}}\cdot E_{\text{rate}}^{\text{uc}}\le E_{t,s}^{\text{uc,st}}\le SOC_{\text{max}}^{\text{uc}}\cdot E_{\text{rate}}^{\text{uc}}\quad\forall t,s \tag{33}$$

$$E_{t=1,s}^{\text{bat,st}}=SOC_{0}^{\text{bat}}\cdot E_{t=1,s}^{\text{bat,act}}\quad\forall s \tag{34}$$

$$E_{t=\text{T},s}^{\text{bat,st}}=SOC_{0}^{\text{bat}}\cdot E_{t=\text{T},s}^{\text{bat,act}}\quad\forall s \tag{35}$$

$$E_{t=1,s}^{\text{uc,st}}=E_{t=\text{T},s}^{\text{uc,st}}=SOC_{0}^{\text{uc}}\cdot E_{\text{rate}}^{\text{uc}}\quad\forall s \tag{36}$$

Equations from (37) to (42) ensure the unique working condition of HESS through binary variables $O_{t,s}^{\text{bat,ch}}$ and $O_{t,s}^{\text{uc,ch}}$. Equation (43) and (44) sum to get the operation time of HESS during a day and feedback to the upper-level model.

$$SOC_{\text{min}}^{\text{bat}}\cdot E_{t,s}^{\text{bat,act}}\le E_{t,s}^{\text{bat,st}}\le SOC_{\text{max}}^{\text{bat}}\cdot E_{t,s}^{\text{bat,act}}\quad\forall t,s \tag{37}$$

$$SOC_{\text{min}}^{\text{uc}}\cdot E_{\text{rate}}^{\text{uc}}\le E_{t,s}^{\text{uc,st}}\le SOC_{\text{max}}^{\text{uc}}\cdot E_{\text{rate}}^{\text{uc}}\quad\forall t,s \tag{38}$$

$$E_{t=1,s}^{\text{bat,st}}=SOC_{0}^{\text{bat}}\cdot E_{t=1,s}^{\text{bat,act}}\quad\forall s \tag{39}$$

$$E_{t=\text{T},s}^{\text{bat,st}}=SOC_{0}^{\text{bat}}\cdot E_{t=\text{T},s}^{\text{bat,act}}\quad\forall s \tag{40}$$

$$E_{t=1,s}^{\text{uc,st}}=E_{t=\text{T},s}^{\text{uc,st}}=SOC_{0}^{\text{uc}}\cdot E_{\text{rate}}^{\text{uc}}\quad\forall s \tag{41}$$

$$SOC_{\text{min}}^{\text{bat}}\cdot E_{t,s}^{\text{bat,act}}\le E_{t,s}^{\text{bat,st}}\le SOC_{\text{max}}^{\text{bat}}\cdot E_{t,s}^{\text{bat,act}}\quad\forall t,s \tag{42}$$

$$SOC_{\text{min}}^{\text{uc}}\cdot E_{\text{rate}}^{\text{uc}}\le E_{t,s}^{\text{uc,st}}\le SOC_{\text{max}}^{\text{uc}}\cdot E_{\text{rate}}^{\text{uc}}\quad\forall t,s \tag{43}$$

$$E_{t=1,s}^{\text{bat,st}}=SOC_{0}^{\text{bat}}\cdot E_{t=1,s}^{\text{bat,act}}\quad\forall s \tag{44}$$

The piecewise linearization method is applied to linearize (26), thus MILP is established at the lower layer. It divides (26) into K segments to get K linear functions of battery cycle loss and cycle depth, which are expressed as (45) and (46). It is noted that K is equal to 16 [37].

$$c(D_{t,s}^{\text{bat}})=\begin{cases}c_1(D_{t,s}^{\text{bat}}) & D_{t,s}^{\text{bat}}\in[0,\frac{1}{K}]\\ \cdots\\ c_k\ (D_{t,s}^{\text{bat}}) & D_{t,s}^{\text{bat}}\in[\frac{k-1}{K},\frac{k}{K}]\\ \cdots\\ c_K(D_{t,s}^{\text{bat}}) & D_{t,s}^{\text{bat}}\in[\frac{K-1}{K},1]\end{cases} \tag{45}$$

$$c_k(D_{t,s}^{\text{bat}})=\frac{c(\frac{k}{K})-c(\frac{k-1}{K})}{K}(D_{t,s}^{\text{bat}}-\frac{k-1}{K})+c(\frac{k-1}{K}) \tag{46}$$

In the PV generation system, the PV power is constrained by the solar intensity $F_{t,s}^{\text{pv}}$ and converter capacity S^{pv}. Likewise, back-to-back converter grid side power and traction side power are also constrained by the converter capacity ($P_{\text{lim}}^{\text{grid}}$ and $P_{\text{lim}}^{\text{fed}}$). In addition, a binary variable $O_{t,s}^{\text{grid}}$ ensures a single working condition of back-to-back converter.

$$P_{t,s}^{\text{pv}}\le 10^{-3}\eta_{\text{pv}}\cdot A_{\text{pv}}\cdot F_{t,s}^{\text{pv}}\quad\forall t,s \tag{47}$$

$$P_{t,s}^{\text{pv}}\le S^{\text{pv}} \tag{48}$$

$$P_{t,s}^{\text{grid}}\le P_{\text{lim}}^{\text{grid}}\cdot O_{t,s}^{\text{grid}}\quad\forall t,s \tag{49}$$

$$P_{t,s}^{\text{fed}}\le P_{\text{lim}}^{\text{fed}}\cdot(1-O_{t,s}^{\text{grid}})\quad\forall t,s \tag{50}$$

IV. Sparrow Search Algorithm with CPLEX Solver Embedded

In this paper, a nonlinear model considering the comprehensive cost is established at the upper layer and solved by SSA, a novel swarm intelligence optimization approach. At the lower layer, CPLEX solver, a large-scale commercial solver, is applied to solve the problem of diurnal FTPSS scheduling, which is formulated as the MILP model.

A. Introduction of SSA

The previous studies have verified the applicability of the heuristic algorithm in optimal energy management [16], [38]. As a novel swarm intelligence optimization approach, SSA is inspired by the behaviors of sparrow. The producers and the scroungers are two different types of captive sparrow house. In order to find food sources more efficiently, both the producer and the scrounger usually participate in the process of predation [24].

Equation (51) uses a matrix to simulate the position of sparrow. Equation (52) represents the fitness value of all sparrows.

$$X=\begin{bmatrix}x_{1,1} & x_{1,2} & \cdots & x_{1,m}\\ x_{2,1} & x_{2,2} & \cdots & x_{2,m}\\ \cdots & \cdots & \cdots & \cdots\\ x_{n,1} & x_{n,2} & \cdots & x_{n,m}\end{bmatrix} \tag{51}$$

$$F_X=\begin{bmatrix}f([x_{1,1} & x_{1,2} & \cdots & x_{1,m}])\\ f([x_{2,1} & x_{2,2} & \cdots & x_{2,m}])\\ \cdots & \cdots & \cdots & \cdots\\ f([x_{n,1} & x_{n,2} & \cdots & x_{n,m}])\end{bmatrix} \tag{52}$$

The location of sparrows is updated to avoid predators or find food sources, which can be expressed in (53).

$$X_{i,j}^{t+1}=\begin{cases} X_{i,j}^{t}\cdot e^{\frac{-i}{\alpha\cdot It_{\max}}} & \mathrm{R}_2 < SST \\ X_{i,j}^{t}+Q_{(1\times \mathrm{m})}\cdot L_{(1\times \mathrm{m})} & \mathrm{R}_2 \geq SST \end{cases} \tag{53}$$

where t is the number of the current iteration. $It_{\max}$ represents the maximum number of iterations. α is a random number from 0 to 1. R_2 is a number from 0 to 1, indicating the alarm value; SST is a number from 0.5 to 1, indicating the safety threshold.

Scroungers will monitor, follow, and compete with the producers when producers find good food. The updated position of scroungers is as follows (54).

$$X_{i,j}^{t+1}=\begin{cases} Q\cdot e^{\frac{X_{\mathrm{worst}}^{t}-X_{\mathrm{i,j}}^{t}}{i^2}} & i>\dfrac{n}{2} \\ X_{P}^{t+1}+\left|X_{i,j}^{t}-X_{i,j}^{t}\right|A^{T}(A_{(1\times \mathrm{m})}A^{T})^{-1}L & i\leq\dfrac{n}{2} \end{cases} \tag{54}$$

where X_{worst}^{t} is the global worst location in iteration t. X_{P}^{t+1} represents the optimal position occupied by the producer in iteration t+1.

The mathematical model of the location updating for sparrows at the edge of the group can be established by (55).

$$X_{i,j}^{t+1}=\begin{cases} X_{\mathrm{best}}^{t}+\beta\cdot\left|X_{\mathrm{i,j}}^{t}-X_{\mathrm{best}}^{t}\right| & f_i>f_g \\ X_{\mathrm{i,j}}^{t}+H\cdot\left(\dfrac{\left|X_{\mathrm{i,j}}^{t}-X_{\mathrm{worst}}^{t}\right|}{(f_i-f_w)+\varepsilon}\right) & f_i=f_g \end{cases} \tag{55}$$

where x_{best}^{t} is the global best location in iteration t. H is a random number from 0 to 1. f_i, f_w and f_g are the present sparrow, which are the current global best and worst fitness values respectively.

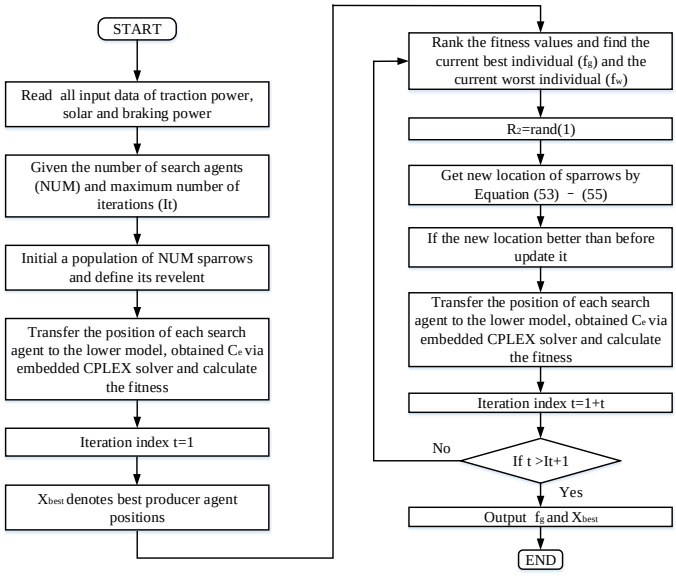

Fig. 7. Follow chart of SSA with CPLEX solver embedded.

B. Application of SSA Approach with CPLEX Solver Embedded

In this paper, the heuristic algorithm SSA is applied to solve nonlinear problems (6). x in (6) is a four-dimensional matrix, representing $P_{\mathrm{rate}}^{\mathrm{bat}}$, $E_{\mathrm{rate}}^{\mathrm{bat}}$, $P_{\mathrm{rate}}^{\mathrm{uc}}$ and $E_{\mathrm{rate}}^{\mathrm{uc}}$ in turn. By inputting various parameters and importing all the required data, Equation (6) works as a function in MATLAB. Then, the maximum number of iterations and population numbers are set, the SSA function is called to solve the above functions, and finally the optimal x is obtained. The SSA first randomly generates x of corresponding population number, as shown in (51), which is the position of sparrow. By substituting x into the lower FTPSS scheduling model, the battery SOC, HESS operation time, and power cost are obtained and returned to the upper layer, and then the comprehensive cost is calculated at the upper layer. The lowest overall cost is found according to (52) to (55), which is also the optimal value in this iteration. The above steps are iterated till convergence so as to obtain the lowest comprehensive cost. Fig. 7 illustrates the overall flowchart of applying SSA and embedded CPLEX solver to achieve the lowest comprehensive cost.

TABLE I
PARAMETERS OF HESS

Parameters	Unit	Battery	UC
PCS costs	CNY/kW	2138	1680
Energy capacity costs	CNY/kWh	3240	61800
Replacement costs	CNY/kWh	1292	28600
BOP costs	CNY/kW	423	423
O&M costs (fixed)	CNY/kW/year	25.5	25.5
O&M costs (variable)	CNY/kW/h	2.78	2.78
Salvage costs	CNY/kW	298	6450
Efficiency (charge/discharge)	—	80%/80%	95%/95%
SOC range	—	20%-80%	5%-95%
Initial SOC	—	50%	50%
Self-discharging rate	/mon	5%	0
Depreciation efficient	—	0.7	0.7

TABLE II
PARAMETERS OF ELECTRICITY CHARGE

Time frames	TOU tariff (CNY/kWh)	Fix tariff (CNY/kWh)
0:00-6:00	0.370	
8:00-11:00	1.252	
18:00-21:00	1.252	0.782
22:00-0:00	0.370	
Others	0.782	

V. CADE STUDY

A. Case Description and Input Parameters

According to the daily operation data of a railway traction substation in reference [16], a detailed case analysis is made. Four different scenarios are adopted, specifically as follows:

Case 1: FTPSS without HESS and PV power generation system is taken as the basic case;

Case 2: FTPSS only connected to PV power generation system;

Case 3: FTPSS only connected to HESS;

Case 4: FTPSS connected to both HESS and PV power generation system;

HESS is composed of lead-acid battery and UC. According to reference [16], the parameters of HESS are shown in Table I, and the engineering cycle and UC lifetime are set as 20 years and 10 years respectively. In this process, only the UC and battery need to be replaced in HESS, and other related devices

are considered to be working during the whole project period. The battery capacity is attenuated and the capacity of UC is constant. Considering the upper bound and lower bound in (16) and (17), (56) is derived.

$$\begin{cases} P_{\text{rate}}^{\text{bat}} \in [1,3]\ \text{MW} \\ E_{\text{rate}}^{\text{bat}} \in [5,10]\ \text{MWh} \\ P_{\text{rate}}^{\text{uc}} \in [10,20]\ \text{MW} \\ E_{\text{rate}}^{\text{uc}} \in [0.1,0.5]\ \text{MWh} \end{cases} \tag{56}$$

As for PV power generation system, it is assumed that $\eta^{\text{pv}}=12\%$, $k_{\text{pv}}=1\,\text{CNY/MW}$ and $A^{\text{pv}}=10^4\text{m}^2$ [39]. PV converter capacity is 1 MVA. Different static pricing schemes including time-of-use (TOU) prices and fixed prices are illustrated in Table II [17]. The demand charge price is 1.2 CNY/kW and annual discount rate r_0 is 5%. This method is implemented under the software environment of MATLAB with the integration of YALMIP toolbox (version 20190425) and IBM ILOG CPLEX solver (version 12.9).

B. Cost Reduction Effect Comparison

Based on the two-part electricity price, it is stipulated that the corresponding penalty should be paid for the power returned to the grid, and the optimal values of each parameter under the time-of-use (TOU) electricity price and the fixed electricity price are obtained. The following cases are analyzed and compared. In case 1, as the basic control group, there is no PV and HESS, and the original costs of TOU and fixed electricity price obtained from Table III are 96.01 k CNY and 108.82 k CNY respectively.

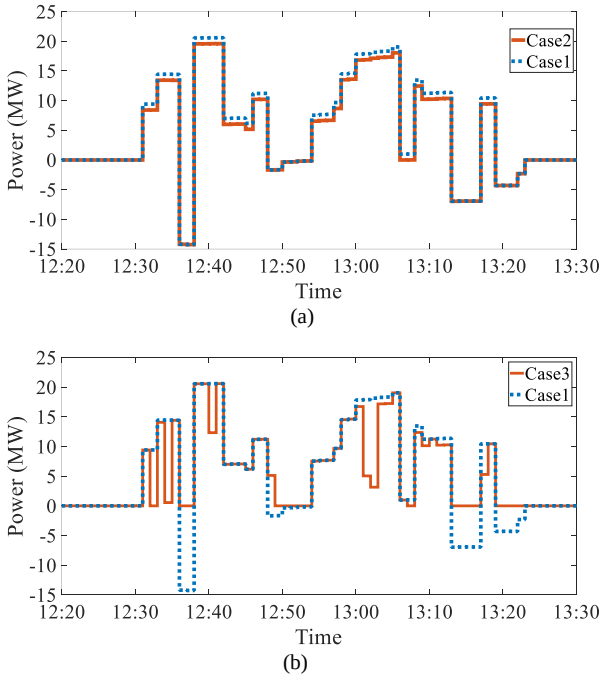

Fig. 8. (a) Power of utility grid in case 1 and case 2 under TOU; (b) Power of utility grid in case 1 and case 3 under TOU.

The electricity cost is slightly higher than the total cost in case 2, because the PV O&M cost is taken into account. When PV is connected, the reduction of the comprehensive cost is 6.61% and 6.65% respectively in the two price schemes. PV can only emit power rather than absorb power, so it can only achieve peak load clipping effect, instead of valley load filling effect. Correspondingly, the PC of Case 1 and Case 2 in Table IV are equal, with a small decrease in DMC. From the grid power ladder diagram in Fig. 8(a), it can be more intuitively observed that only the peak load is reduced.

In case 3, peak load shaving and valley load filling are realized by the charge and discharge of HESS. However, considering the total cost of the HESS and under different price schemes, the electricity charge reduction rates in case 3 are 4.06% and 5.55% respectively. It can be further confirmed from Fig. 8(b) that HESS can complete peak load shaving and restraining volatility well. According to Table IV, the PC in case 3 is almost zero, which is significantly lower than that in case 2 and case 1. This indicates that HESS can fully absorb the RBE generated by the train and improve the utilization rate of RBE. In addition, according to the energy conservation constraint (25), the RBE absorbed by HESS is used to provide train traction and reduce ECC and DMC.

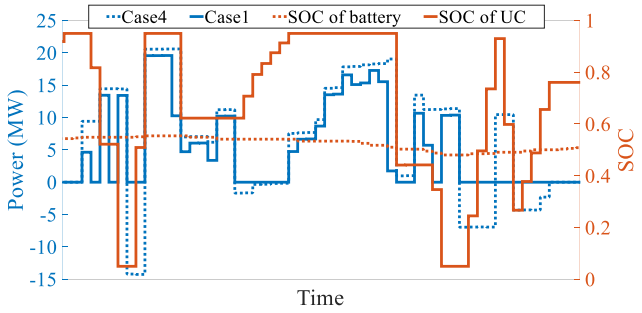

Fig. 9. Power of utility grid in case 1 and case 4 under TOU, SOC of LA battery and UC in case 4 under TOU.

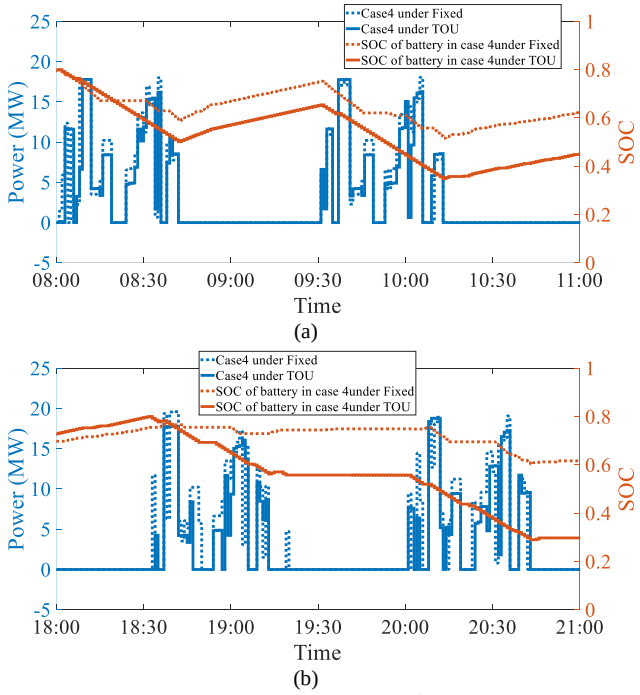

Fig. 10. (a) Optimal results at 8:00 to 11:00: power of utility grid in case 4 under TOU and Fixed, SOC of LA battery in case4 under TOU and Fixed. (b) Optimal results at 18:00 to 21:00: power of utility grid in case 4 under TOU and Fixed, SOC of LA battery in case4 under TOU and Fixed.

In case 4, under different electricity prices, the total cost reduction increases to 10.48% and 13.55%, respectively. Fig. 9 shows that the SOC of the battery is very gentle, while UC is

TABLE III
RESULTS OF DIFFERENT CASES

Cases	Caes1		Case2		Case3		Case4	
Pricing Schemes	Fixed Tariff	TOU Tariff	Fixed Tariff	TOU Tariff	Fixed Tariff	TOU Tariff	Fixed Tariff	TOU Tariff
$P_{\text{rate}}^{\text{bat}}$ /MW	—	—	—	—	1.46	1.1	2.5	1.7
$E_{\text{rate}}^{\text{bat}}$ /MWh	—	—	—	—	5.0	5.0	5.0	5.0
$P_{\text{rate}}^{\text{uc}}$ /MW	—	—	—	—	10.06	13.9	14.8	14.6
$E_{\text{rate}}^{\text{uc}}$ /MWh	—	—	—	—	0.386	0.5	0.46	0.49
T_{bat} /year	—	—	—	—	**5.44**	**4.12**	**2.62**	**2.49**
C_{e} /k CNY	96.01	108.82	89.65	101.57	72.4	78.77	58.73	66.13
$C_{\text{HESS}}^{\text{cap}}$ /k CNY	—	—	—	—	12.00	14.58	15.13	15.02
$C_{\text{HESS}}^{\text{rep}}$ /k CNY	—	—	—	—	5.622	7.39	10.75	12.10
$C_{\text{HESS}}^{\text{om}}$ /k CNY	—	—	—	—	1.57	2.05	2.36	2.23
C_{sal} /k CNY	—	—	—	—	14.17	5.06	0.27	1.41
C_{total} /k CNY	96.01	108.82	89.66	101.58	92.11	102.78	86.94	94.07
Electricity Cost Savings	—	—	6.62%	6.66%	24.59%	27.61%	38.83%	39.23%
Total Cost Savings	—	—	6.61%	6.65%	4.06%	5.55%	**10.48%**	**13.55%**

TABLE IV
ELECTRICITY COST IN DIFFERENT CASES

Cases	Case 1		Case 2		Case 3		Case 4	
Cost /k CNY	Fixed Tariff	TOU Tariff	Fixed Tariff	TOU Tariff	Fixed Tariff	TOU Tariff	Fixed Tariff	TOU Tariff
ECC	66.96	78.22	62.65	73.02	58.83	66.01	48.05	54.83
DC	17.37	17.37	16.16	16.16	12.89	12.47	10.43	11.12
PC	10.85	12.40	10.85	12.40	1.03	0.19	0.24	0.18
C_e	96.01	108.82	89.68	101.57	72.4	78.77	58.73	66.13

frequently charged and discharged. As a large-capacity energy storage device, batteries can store energy and corresponding low-frequency power. As a high-power energy storage device, UC frequently charges, discharges and responds to high-frequency power. In addition, the peak cutting of power grid is always accompanied by the discharge of UC, and the valley filling of power is always accompanied by the charging of UC.

Based on the comprehensive comparison of the four cases, it can be found that the access to PV and HESS in case 4 can achieve the maximum cost reduction. Compared with other cases, the PC, DMC and ECC in case 4 are also the lowest, which indicates that HESS makes good use of PV and RBE and reduces electricity costs while improving PV and RBE utilization rates.

C. Battery Lifetime Distribution in Different Cases

According to T_{bat} in Table III, the battery life varies under different pricing strategies and in different cases. The battery lifetime shows such a rule: the battery life under the fixed tariff is longer than that under the TOU tariff. For example, the battery life under the TOU tariff in case 3 is 4.12 years while the battery life under the fixed tariff is 5.44 years, which is due to the high TOU electricity price during the peak period of electricity consumption. Batteries will release more electricity in the peak period than in the fixed period, thus reducing the electricity price to a greater extent. The SOC of the battery under TOU tariff is lower than that under fixed tariff in Fig. 10, which indicates that the battery will release more electricity at the cost of reduced battery life during the period from 8:00 to 11:00 so as to achieve lower electricity cost. In the three hours from 8:00 to 11:00, the two price schemes in case 4 have the same price reduction effect, and both prices reduce by 28.71%, which also shows that the battery releases more energy at the peak of TOU tariff at the cost of sacrificing life.

In Table III, due to the PV access, the battery life of case 4 is generally lower than that in case 3 when the same price scheme is adopted. The HESS will store part of the solar energy to better cut peak load and fill valley load, thereby reducing battery life.

D. Battery Capacity Degradation Comparison

In this paper, the piecewise linearization method is adopted. According to Fig. 11(a), the degradation degree of battery capacity decreases with the increase of piece, but the decreasing trend gradually flattens out. Starting from about 10, the range of battery capacity degradation becomes smaller and smaller. Therefore, considering the calculation time, K is taken as 16 in this paper.

The model without considering battery capacity degradation was selected as the comparison object [16]. Fig. 11(b) shows the battery capacity attenuation curves of the two models. The battery capacity attenuation rate of proposed model is slower than that of model without considering battery capacity

degradation. When the battery capacity degradation is not considered, the battery will be charged and discharged as much as possible to achieve the function of peak clipping and valley filling. However, each charge and discharge of the battery will lead to the decay of the battery capacity, so the battery capacity decay rate is slowed down when the battery capacity degradation is taken as the constraint.

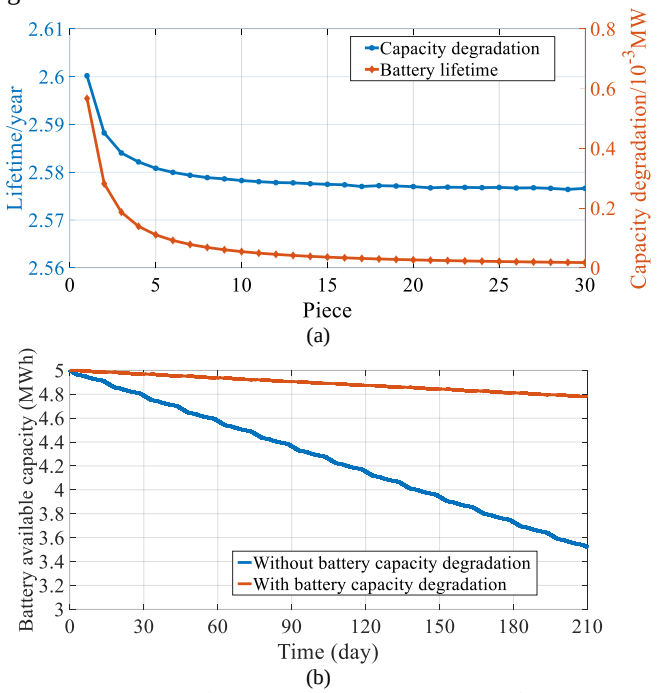

Fig. 11. (a) The curves of battery capacity degradation and lifetime changing with piece. (b) The battery capacity decline curve over 15 days.

E. Comparison of Different Models and Algorithms

In order to evaluate the performance and advantages of the proposed two-layer scheduling model, the proposed model is compared with the simplified MILP model [9] and the nonlinear bi-level model [16]. The maximum number of daily battery cycles for the simplified MILP model is set to 10. Table V shows the results of the comparative models in case 4 under TOU. As shown in Table V, the proposed model obtains the lowest total cost and reduces the cost by 13.55%, while the simplified MILP model and nonlinear bi-level model reduce the cost by 9.69% and 12.29%, respectively. The battery degradation model is simplified and a linear model is established in reference [9], which has faster solving speed but lower accuracy. In contrast, based on the number of battery cycles and DOD curve, the battery degradation model is established in reference [16], and the intelligent algorithm is used to solve the nonlinear model, so as to get a lower comprehensive cost. The battery capacity degradation is considered in the proposed model and the lowest cost is got by optimizing the HESS parameters.

In the upper model, SSA is applied to solve nonlinear problems. As widely used intelligent algorithms, GWO and modified particle swarm optimization (MPSO) [40] have a strong application foundation. However, SSA, as a newly proposed algorithm, has more development potential. SSA, GWO, and MPSO are compared in terms of iteration times and optimization accuracy. Three algorithms optimized case 3 with the same parameters. Table VI and Fig. 12 show the faster convergence speed and higher accuracy of SSA, which converges to 92.11k in the tenth iteration. In addition, the optimization result of SSA in the first iteration is significantly lower than that of the other two algorithms, which demonstrates the excellent initial optimization ability of SSA.

TABLE V
RESULTS OF DIFFERENT MODELS IN CASE 4 UNDER TOU

Models	P_{rate}^{bat} /MW	E_{rate}^{bat} /MWh	P_{rate}^{uc} /MW	E_{rate}^{uc} /MWh	C_{total} /k CNY	Cost saving
Simplified MILP model	2.4	5.4	18.5	0.48	98.28	9.69%
Nonlinear bi-level model	2.5	5.0	15.4	0.50	95.45	12.29%
Proposed two-layer model	1.7	5.0	14.6	0.49	94.07	13.55%

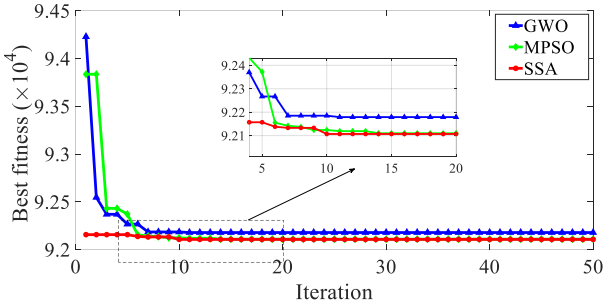

Fig. 12. Iterative curves for different algorithms.

TABLE VI
CONVERGENCE CHARACTERISTICS OF DIFFERENT ALGORITHMS FOR CASE 3 UNDER FIXED TARIFF

Parameters	GWO	MPSO	SSA
Iterations	11	16	10
Value($\times 10^4$)	9.218	9.211	9.211

F. Sensitivities Analysis

Fig. 13 shows the variation trend of total cost, HESS investment cost and cost reduction effect as the project period increases. As Fig. 13 shows, the proposed method pays for itself in the eighth year and becomes profitable each year thereafter. When the project period is 20 years, the total cost saving is 13.55%.

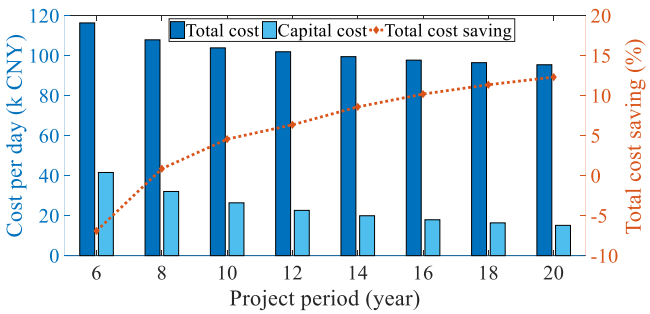

Fig. 13. The impact of project period on cost saving.

VI. CONCLUSION

In this paper, the FTPSS integrated with HESS and PV is studied. Considering the engineering cycle and daily scheduling, the FTPSS two-layer scheduling optimization model is proposed. In the upper layer, the comprehensive life

cycle cost and replacement strategy of HESS are achieved, and HESS capacity and power are optimized. In the lower layer, the online battery capacity degradation model is established with respect to the depth of discharge (DOD), and optimized power flow control strategy of back-to-back converter is given for minimum electricity charge. Finally, the SSA algorithm embedded in CPLEX solver is introduced to solve the two-layer nonlinear model.

Case study shows that the energy management of FTPSS reduces the railway operating cost by 10.48% and 13.55% under fixed tariff and TOU, respectively. The model proposed in this paper can effectively slow down the rate of battery capacity degradation. For the nonlinear model proposed in this paper, SSA has higher accuracy and faster convergence speed than GWO and MPSO.

REFERENCES

[1] X. Zhu, H. Hu, H. Tao, and Z. He, "Stability Analysis of PV Plant-Tied MVdc Railway Electrification System," IEEE Transactions on Transportation Electrification, vol. 5, no. 1, pp. 311-323, 2019.

[2] Y. Chen, M. Chen, Z. Tian, Y. Liu, and S. Hillmansen, "VU limit pre-assessment for high-speed railway considering a grid connection scheme," IET Generation, Transmission & Distribution, vol. 13, no. 7, pp. 1121-1131, 2019.

[3] I. Krastev, P. Tricoli, S. Hillmansen, and M. Chen, "Future of electric railways: advanced electrification systems with static converters for ac railways," IEEE Electrification Magazine, vol. 4, no. 3, pp. 6-14, 2016.

[4] E. P. de la Fuente, S. K. Mazumder, and I. G. Franco, "Railway Electrical Smart Grids: An introduction to next-generation railway power systems and their operation," IEEE Electrification Magazine, vol. 2, no. 3, pp. 49-55, 2014.

[5] X. He et al., "Advanced cophase traction power supply system based on three-phase to single-phase converter," IEEE Transactions on Power Electronics, vol. 29, no. 10, pp. 5323-5333, 2013.

[6] S. D'Arco, L. Piegari, and P. Tricoli, "Comparative Analysis of Topologies to Integrate Photovoltaic Sources in the Feeder Stations of AC Railways," IEEE Transactions on Transportation Electrification, vol. 4, no. 4, pp. 951-960, 2018.

[7] X. Shen, H. Wei, and T. T. Lie, "Management and Utilization of Urban Rail Transit Regenerative Braking Energy based on the Bypass DC Loop," IEEE Transactions on Transportation Electrification, pp. 1-1, 2020.

[8] G. Cui et al., "Supercapacitor Integrated Railway Static Power Conditioner for Regenerative Braking Energy Recycling and Power Quality Improvement of High-Speed Railway System," IEEE Transactions on Transportation Electrification, vol. 5, no. 3, pp. 702-714, 2019.

[9] S. de la Torre, A. J. Sanchez-Racero, J. A. Aguado, M. Reyes, and O. Martianez, "Optimal Sizing of Energy Storage for Regenerative Braking in Electric Railway Systems," IEEE Transactions on Power Systems, vol. 30, no. 3, pp. 1492-1500, 2015.

[10] C. Wu, B. Xu, S. Lu, F. Xue, and M. Chen, "Adaptive Eco-Driving Strategy and Feasibility Analysis for Electric Trains with On-Board Energy Storage Devices," IEEE Transactions on Transportation Electrification, 2021.

[11] H. Yu, Y. Wang, and Z. Chen, "A Novel Renewable Microgrid-enabled Metro Traction Power System -Concepts, Framework and Operation Strategy," IEEE Transactions on Transportation Electrification, pp. 1-1, 2021.

[12] F. Naseri, E. Farjah, Z. Kazemi, E. Schaltz, T. Ghanbari, and J.-L. Schanen, "Dynamic Stabilization of DC Traction Systems Using a Supercapacitor-Based Active Stabilizer With Model Predictive Control," IEEE Transactions on Transportation Electrification, vol. 6, no. 1, pp. 228-240, 2020.

[13] H. Novak, V. Lesic, and M. Vasak, "Hierarchical Model Predictive Control for Coordinated Electric Railway Traction System Energy Management," IEEE Transactions on Intelligent Transportation Systems, vol. 20, no. 7, pp. 2715-2727, 2019.

[14] I. Sengor, H. C. Kilickiran, H. Akdemir, B. Kekezoglu, O. Erdinc, and J. P. S. Catalao, "Energy Management of a Smart Railway Station Considering Regenerative Braking and Stochastic Behaviour of ESS and PV Generation," IEEE Transactions on Sustainable Energy, vol. 9, no. 3, pp. 1041-1050, 2018.

[15] J. A. Aguado, A. J. S. Racero, and S. D. L. Torre, "Optimal Operation of Electric Railways With Renewable Energy and Electric Storage Systems," IEEE Transactions on Smart Grid, vol. 9, no. 2, pp. 993-1001, 2018.

[16] Y. Liu, M. Chen, S. Lu, Y. Chen, and Q. Li, "Optimized sizing and scheduling of hybrid energy storage systems for high-speed railway traction substations," Energies, vol. 11, no. 9, p. 2199, 2018.

[17] M. Chen, Z. Cheng, Y. Liu, Y. Cheng, and Z. Tian, "Multitime-Scale Optimal Dispatch of Railway FTPSS Based on Model Predictive Control," IEEE Transactions on Transportation Electrification, vol. 6, no. 2, pp. 808-820, 2020.

[18] Y. Liu, M. Chen, Z. Cheng, Y. Chen, and Q. Li, "Robust Energy Management of High-Speed Railway Co-Phase Traction Substation With Uncertain PV Generation and Traction Load," IEEE Transactions on Intelligent Transportation Systems, pp. 1-13, 2021.

[19] Q. Li et al., "Online extremum seeking-based optimized energy management strategy for hybrid electric tram considering fuel cell degradation," Applied Energy, vol. 285, 2021.

[20] Z. Pan, M. Chen, S. Lu, Z. Tian, and Y. Liu, "Integrated Timetable Optimization for Minimum Total Energy Consumption of an AC Railway System," IEEE Transactions on Vehicular Technology, vol. 69, no. 4, pp. 3641-3653, 2020.

[21] Z. Hou, H. Dong, S. Gao, G. Nicholson, L. Chen, and C. Roberts, "Energy-Saving Metro Train Timetable Rescheduling Model Considering ATO Profiles and Dynamic Passenger Flow," IEEE Transactions on Intelligent Transportation Systems, vol. 20, no. 7, pp. 2774-2785, 2019.

[22] Q. Li, L. Yin, H. Yang, T. Wang, Y. Qiu, and W. Chen, "Multi-Objective Optimization and Data-Driven Constraint Adaptive Predictive Control for Efficient and Stable Operation of PEMFC System," IEEE Transactions on Industrial Electronics, pp. 1-1, 2020.

[23] R. Su, Q. Gu, and T. Wen, "Optimization of High-Speed Train Control Strategy for Traction Energy Saving Using an Improved Genetic Algorithm," Journal of Applied Mathematics, vol. 2014, pp. 1-7, 2014.

[24] J. Xue and B. Shen, "A novel swarm intelligence optimization approach: sparrow search algorithm," Systems Science & Control Engineering, vol. 8, no. 1, pp. 22-34, 2020.

[25] H. Dong, S. Li, H. Dong, Z. Tian, and S. Hillmansen, "Coordinated Scheduling Strategy for Distributed Generation Considering Uncertainties in Smart Grids," IEEE Access, vol. 8, pp. 86171-86179, 2020.

[26] B. Xu, A. Oudalov, A. Ulbig, G. Andersson, and D. S. Kirschen, "Modeling of Lithium-Ion Battery Degradation for Cell Life Assessment," IEEE Transactions on Smart Grid, vol. 9, no. 2, pp. 1131-1140, 2018.

[27] Q. Li, W. Yang, L. Yin, and W. Chen, "Real-Time Implementation of Maximum Net Power Strategy Based on Sliding Mode Variable Structure Control for Proton-Exchange Membrane Fuel Cell System," IEEE Transactions on Transportation Electrification, vol. 6, no. 1, pp. 288-297, 2020.

[28] C. Amzallag, J. P. Gerey, J. L. Robert, and J. Bahuaud, "Standardization of the rainflow counting method for fatigue analysis," International Journal of Fatigue, vol. 16, no. 4, pp. 287-293, 1994.

[29] C. Ju, P. Wang, L. Goel, and Y. Xu, "A Two-Layer Energy Management System for Microgrids With Hybrid Energy Storage Considering Degradation Costs," IEEE Transactions on Smart Grid, vol. 9, no. 6, pp. 6047-6057, 2018.

[30] G. Alcicek, H. Gualous, P. Venet, R. Gallay, and A. Miraoui, "Experimental study of temperature effect on ultracapacitor ageing," in European Conference on Power Electronics & Applications, 2008.

[31] D. Linzen, S. Buller, E. Karden, and R. W. D. Doncker, "Analysis and Evaluation of Charge-Balancing Circuits on Performance, Reliability, and Lifetime of Supercapacitor Systems," IEEE Transactions on Industry Applications, vol. 41, no. 5, pp. 1135-1141, 2005.

[32] D. Roch-Dupre, A. J. Lopez-Lopez, R. R. Pecharroman, A. P. Cucala, and A. Fernandez-Cardador, "Analysis of the demand charge in DC railway systems and reduction of its economic impact with Energy Storage Systems," International Journal of Electrical Power & Energy Systems, vol. 93, no. dec., pp. 459-467, 2017.

[33] A. Suresh, S. J. Hossain, S. Abdelrazek, and S. Kamalasadan, "Online Power Profile Based Universal Battery Degradation Methodology

Suitable for Various Battery Types," in 2019 IEEE Power & Energy Society General Meeting (PESGM), 2019.
[34] D. Shen, T. Xu, L. Wu, and Y. Guan, "Research on Degradation Modeling and Life Prediction Method of Lithium-ion Battery in Dynamic Environment," IEEE Access, vol. PP, no. 99, pp. 1-1, 2019.
[35] I. Laresgoiti, S. Kaebitz, M. Ecker, and D. U. Sauer, "Modeling mechanical degradation in lithium ion batteries during cycling: Solid electrolyte interphase fracture," Journal of Power Sources, vol. 300, no. DEC.30, pp. 112-122, 2015.
[36] H. Farzin, M. Fotuhi-Firuzabad, and M. Moeini-Aghtaie, "A Practical Scheme to Involve Degradation Cost of Lithium-Ion Batteries in Vehicle-to-Grid Applications," IEEE Transactions on Sustainable Energy, vol. 7, no. 4, pp. 1730-1738, 2016.
[37] B. Xu, J. Zhao, T. Zheng, E. Litvinov, and D. S. Kirschen, "Factoring the Cycle Aging Cost of Batteries Participating in Electricity Markets," IEEE Transactions on Power Systems, vol. PP, no. 99, pp. 1-1, 2017.
[38] S. Sharma, S. Bhattacharjee, and A. Bhattacharya, "Grey wolf optimisation for optimal sizing of battery energy storage device to minimise operation cost of microgrid," IET Generation, Transmission & Distribution, vol. 10, no. 3, pp. 625-637, 2016.
[39] M. A. Green, K. Emery, Y. Hishikawa, W. Warta, and E. D. Dunlop, "Solar cell efficiency tables (version 43)," Progress in Photovoltaics: Research and Applications, vol. 22, no. 1, pp. 1-9, 2014.
[40] Y. Chen, F. Lou, Y. Jiang, Q. Ye, N. Wang, and G. Ying, "A Modified Particle Swarm Optimization Based Algorithm for the Energy Management Strategy of a Regional Integrated Energy System," presented at the 2020 IEEE 9th International Power Electronics and Motion Control Conference (IPEMC2020-ECCE Asia), 2020.

Minwu Chen (M'17) received the B.Eng. and Ph.D. degrees in electrical engineering from Southwest Jiaotong University, Chengdu, China, in 2004 and 2009, respectively.
From 2010 to 2012, he undertook postdoctoral researches in the China Railway First Survey and Design Institute Group, Xi'an, China. Since 2018, he has been a Full Professor at the School of Electrical Engineering, Southwest Jiaotong University, Chengdu, China. From 2014 to 2015, he was a Visiting Scholar at the University of Birmingham, Birmingham, UK. His research interests include new technology and power quality for railway traction systems.

Zongyou Liang received the B.Eng. degree in the School of Electrical Engineering from Southwest Jiaotong University, Chengdu, China, in 2020, where he is currently working toward the M.Eng. degree in the School of Electrical engineering, Southwest Jiaotong University. His primary research interests is the optimal operation and planning for the integration of renewable energy and storage in high-speed railway system.

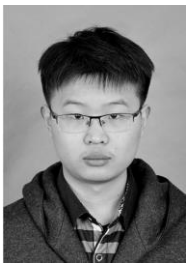

Zhe Cheng received the B.Eng. degree in smart grid information engineering from Qingdao University of Science and Technology, Qingdao, China, in 2018, He received the M.Eng. degree in electrical engineering from Southwest Jiaotong University, Chengdu, China, in 2021. His current research interest is the energy management of electric railway system integrated energy storage and renewable energy.

Jinyu Zhao received the B.Eng. degree in Electrical Engineering and Automation from Inner Mongolia University of Technology, Hohhot, China, in 2020. He is currently working toward the M.Eng. degree in electrical engineering from Southwest Jiaotong University, Chengdu, China. His current research interest is the electromagnetic interference of traction power supply system, power quality and renewable energy.

Zhongbei Tian received the B.Eng. in Huazhong University of Science and Technology, Wuhan, China, in 2013. He received the B.Eng. and Ph.D. degree in Electrical and Electronic Engineering from the University of Birmingham, Birmingham, U.K., in 2013 and 2017. He is currently a Lecturer in Electrical Energy Systems at the University of Liverpool. His research interests include railway traction power system modeling and analysis, energy-efficient train control, energy system optimization, and sustainable transport energy systems integration and management.